

Effect of magnetic field on the burning of a neutron star

Ritam Mallick* and Amit Singh

Indian Institute of Science Education and Research Bhopal, Bhopal, India

(Dated: September 6, 2018)

Abstract

In this article we present the effect of strong magnetic field in the burning of neutron star (NS). We have used relativistic magneto-hydrostatic (MHS) conservation equations for studying the PT from nuclear matter (NM) to quark matter. We have assumed the matter to be infinitely conducting and had solved our equations in the de-Hoffmann Teller (HT) frame for mathematical simplicity. Our nuclear and quark EoSs satisfies the current bound on the pulsar mass measurement. We have seen that the shock induced phase transition (PT) is likely if the density of the star core is more than 3 times nuclear saturation (ρ_s) density. We have also found that the conversion process from NS to quark star (QS) is always an exothermic process. The PT at the center always starts as a slow deflagration, when there is a slight density and pressure fluctuation at the center of the star. We also found that usually for small infalling matter velocities at the star core, the magnetic field in the quark phase (QP) is less than that of the nuclear phase (NP) just after the PT. We also infer that for large enough baryon density and infalling matter velocity, the tilt in the magnetic axis of the star with respect to star's body axis changes considerably. Finally, we found that in such astrophysical PT scenario time-like shock is difficult to initiate at the stars core.

PACS numbers: 47.40.Nm, 52.35.Tc, 26.60.Kp, 97.10.Cv

Keywords: dense matter, equation of state, stars : magnetic field, stars: neutron, shock waves

* mallick@iiserb.ac.in

I. INTRODUCTION

One of the most challenging aspect in astrophysics is the study and understanding of compact objects. Compact objects usually refers to the family of white dwarfs, compact stars and black hole, which are formed after the gravitational collapse of a dead star. Among the compact objects compact stars (otherwise commonly known as neutron stars (NS) or quark stars (QS)) has a special significance in astrophysics because in addition to the importance of the objects themselves they also serves as a tool to improve the understanding of nuclear matter (NM) and possibly quark matter (QM) at very large densities and low temperatures (see e.g. [1, 2]). Thus the compact star serves as an ideal complementary approach to the study of high temperature relativistic heavy-ion collisions.

Our understanding of compact stars has changed in the last fifty years, beginning with the discovery of pulsars [3] and connecting them with NS [4] . It was quite well understood that pulsars are nothing but spinning compact stars (CS) emitting mostly x-rays and radio waves. The central density of CS are inferred to be as high as 3–10 times nuclear saturation density. Over time various equation of state (EoS) of matter at such high density has been proposed and is being continuously refined. One of the most exciting aspect which arose from such high density stars is the occurrence of QM in their cores where confinement to deconfinement transition takes place, resulting in QS. Therefore, CS can be of two types a) NS composed entirely of NM
b) QS which have some quantity of denconfined QM in them.

While the nuclear and quark model has improved over years, major advancement came from the astrophysical observation.

The change has been more rapid in the last decade, when the discovery and timing observation of pulsars has gained acceleration due to the advent of new generation of space-based X-ray and gamma-ray satellites (Einstein/EXOSAT). Important observation also came from the ROSAT observatory. However, a totally new era of thermal radiation observation started after the launching of CHANDRA and XMM-Newton Observatory. With improved telescopes and interferometric techniques the number of observed binary pulsars is continuously increasing. Till date we have the knowledge of precise masses of about 35 pulsars spanning the range from $1.15M_{\odot}$ to $2.01M_{\odot}$. The radius measurement is not as precise as the masses, however, it is widely accepted that they must lie in the range between 9 – 12 km.

The knowledge of heaviest NS, PSR J1614-2230 and PSR J0348+0432 [5, 6] and connecting them with the existing radius bound already places a significant constraint on the EoS of matter at these extreme densities.

The possible existence of both NS and QS has been proposed long back [7–9]. The conversion of a NS to a QS is likely through a deconfined phase transition (PT). The PT can occur either soon after the formation of the NS in a supernovae explosion or during the later time through a first order PT. The phase transformation is usually assumed to begin at the center of a star when the density increases beyond the critical density. The PT can be triggered by several processes: slowing down of the rotating star [10], accretion of matter on the stellar surface [11] or simply cooling. Such a PT should be characterized by a significant energy release in the form of latent heat, which will be accompanied by a neutrino burst, thereby cooling the star. Corresponding star transformations should lead to interesting observable signatures like γ -ray bursts [12–15], changes in the cooling rate [16], and the gravitational wave (GW) emission [17].

The dynamical study of PT is rather uncertain and even controversial [18]. In the literature one can find two very different scenarios: (i) the PT is a slow deflagration process and never a detonation [19] and (ii) the PT from confined to deconfined matter is a fast detonation-like process, which lasts about 1 ms [20]. If the process is fast burning and very violent (detonation) there could be very strong GW signals coming from them which could be detected at least in the second or third generation of VIRGO and LIGO GW detectors [17, 21]. The most early calculation [22] assumed the conversion to proceed via a slow combustion, where the conversion process depends strongly on the temperature of the star. Later [23] studies the stability of the conversion process, and found that under the influence of gravity the conversion process becomes unstable and the slow combustion can become a fast detonation. Relativistic calculation was done [24] to determine the nature of the conversion process, employing the energy momentum conservation and baryon number conservation (also known as rankine-hugoniot condition). However, there is still no consensus about the nature of the conversion process.

Another unique feature of compact stars is the presence of ultra strong magnetic field in their surface. The surface field strength in almost all pulsars are of the order of $10^8 - 10^{12}$ G. However, recent observations of several new pulsars, namely some anomalous X-ray pulsars (AXP) and soft-gamma repeaters (SGR), have been identified to have much stronger surface

magnetic fields [25, 26]. Such pulsars with strong magnetic fields are separately termed as magnetars [27, 28]. Such field are usually estimated from the observation of the NS period and the period derivative. It has also been attributed that the observed giant flares, SGR 0526-66, SGR 1900+14 and SGR 1806-20 (Palmer et al. 2005), are the manifestation of such strong surface magnetic in those stars. While magnetic fields as high as 10^{15} G have been inferred at the surface of magnetars [27, 29, 30], there is indirect evidence for fields as high as 10^{16} G inside the star [31].

The origin of such high magnetic field is still unknown. The magnetic field of regular old pulsars can be attributed to the conservation of the magnetic flux during the core collapse of a supernovae. However, they are unable to explain the strong surface fields of magnetars. The idea by Thompson and Duncan [27], suggest a dynamo process by combining convection and differential rotation in hot proto-neutron stars can build up field of strength of 10^{15} G. Recently it was suggested that magneto-rotational instability and MRI driven dynamo in hot proto-neutron stars can amplify normal magnetic field strength to very high values in quite short time [32–36]. Whatever may be the origin of such magnetic fields it is clear that they would have significant impact on the physical aspect of such stars.

The aim of this present work is to study the effect of such strong magnetic field in the conversion of NS to QS. Instead of using the relativistic conservation condition we would employ MHS conservation condition in the HT frame [37]. We will treat the matter as an ideal fluid with an infinite conductivity. We would mostly concern ourselves with the space-like shocks, where the shock propagates with a velocity less than the speed of light. However, in some situations there may be a fast PT (first order) where the normal vector to the surface of the discontinuity can be time-like [38]. It was argued that a system undergoing rapid and homogeneous rarefaction, bubbles at different spatial points are formed which are causally unconnected to each other. For such cases the phase boundary separating the two phases of matter becomes time-like. Although it is difficult to realize time-like shocks in the astrophysical scenario we would be interested in its theoretical implication if any.

In our investigation we would assume that a the PT takes place inside a cold β stable NS. We assume that the formation of the new phase takes place at the center of the star due to sudden fluctuation of the star density. The star then burns from the core to the periphery. The conversion process would be determined by the conservation equations and the EoS of the matter on either side of the front. As the new phase reaches the boundary it slows down

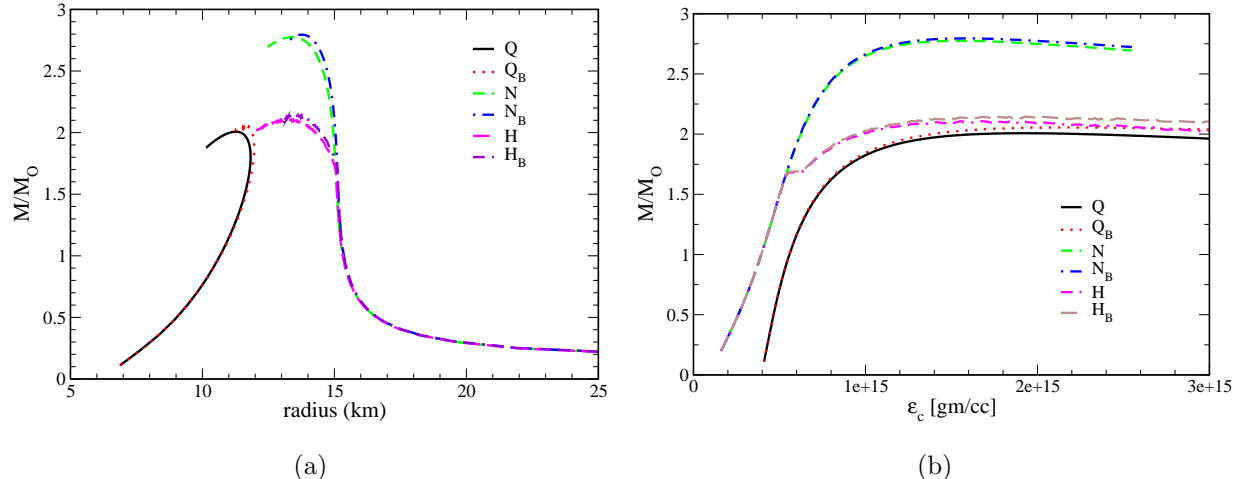


FIG. 1. (Color online) a) The mass-radius sequence of different compact stars (NS, QS and HS) obtained by solving the TOV equations. Also shown in the graphs are the mass-radius sequence of axisymmetric magnetized stars. b) The mass-energy sequence for the same family of the stars for showing the unstable sequence. Quantities with subscript B is for magnetized stars (or magnetars).

as the density decreases. It may even stop at some point inside the star.

The paper is organized as followed. In section 2 we discuss the EoS of star before and after the PT keeping in mind the recent observational bound. The initial star is of hadronic matter whereas the final burned state is of deconfined QM. In section 3 we discuss about the effect of magnetic field on the star structure. Next, in section 4 we discuss the MHS conservation equation for the space-like and time-like conversion front. In section 5 we show our main results aiming to clarify and classify the conversion process. Finally in section 6 we summarize our findings and discuss about their potential astrophysical implications.

II. EOS FOR NS AND QS

The PT is brought about by a sudden density fluctuation at the star core. This initiates a finite density and pressure fluctuation which propagates outwards. This fluctuation is assumed to propagate along a single very thin layer, known as PT front, converting NM to QM. Therefore, to describe the properties of NM and QM we need EoSs. We employ such EoSs which satisfies the current bound on the recent pulsar mass measurement. We use zero temperature EoS as we assume that the PT takes place due to density fluctuation in any normal cold pulsars. However, the final burnt QM can have finite temperature depending

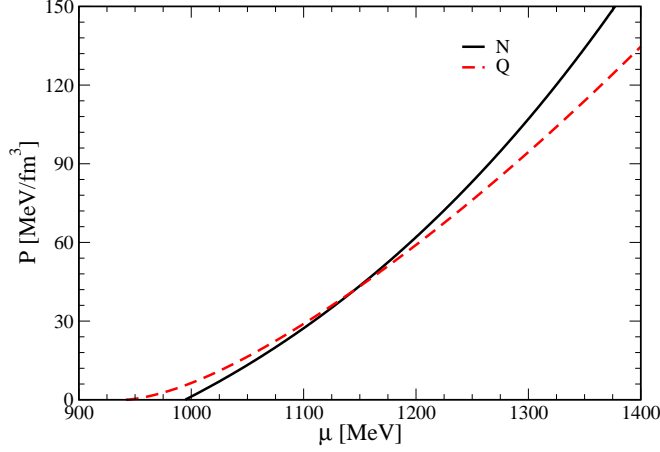


FIG. 2. (Color online) Pressures of (NM) and (QM) as functions of baryon chemical potential. N stands for NM and Q for QM. The intersection point corresponds to the equilibrium PT from NM to QM.

on the EoS of matter on either side of the PT front. For the hadronic phase we adopt a relativistic mean field approach which is generally used to describe the NM in CS. The corresponding Lagrangian is given in the following form [39–41] ($\hbar = c = 1$)

$$\begin{aligned} \mathcal{L}_H = & \sum_n \bar{\psi}_n [\gamma_\mu (i\partial^\mu - g_{\omega n} \omega^\mu - \frac{1}{2} g_{\rho n} \vec{\tau} \cdot \vec{\rho}^\mu) - (m_n - g_{\sigma n} \sigma)] \psi_n \\ & + \frac{1}{2} (\partial_\mu \sigma \partial^\mu \sigma - m_\sigma^2 \sigma^2) - \frac{1}{3} b \sigma^3 - \frac{1}{4} c \sigma^4 - \frac{1}{4} \omega_{\mu\nu} \omega^{\mu\nu} + \\ & \frac{1}{2} m_\omega^2 \omega_\mu \omega^\mu - \frac{1}{4} \vec{\rho}_{\mu\nu} \cdot \vec{\rho}^{\mu\nu} + \frac{1}{2} m_\rho^2 \vec{\rho}_\mu \cdot \vec{\rho}^\mu + \sum_l \bar{\psi}_l [i\gamma_\mu \partial^\mu - m_l] \psi_l. \end{aligned} \quad (1)$$

The EoS contains only nucleons (n) and leptons ($l = e^\pm, \mu^\pm$). The leptons are assumed to be non-interacting, but the nucleons interacts with the scalar σ mesons, the isoscalar-vector ω_μ mesons and the isovector-vector ρ_μ mesons. The basic properties of NM and that of finite nuclei are used to fit the adjustable parameter of the model. In our present calculation we use NL3 parameter set [42], which usually generates massive NSs.

To describe the QM we use simple MIT bag model [43]. The inclusion of the quark interaction in this basic model makes it possible to satisfy the present mass bound. The grand potential of the model is given by

$$\Omega_Q = \sum_i \Omega_i + \frac{\mu^4}{108\pi^2} (1 - a_4) + B \quad (2)$$

where i stands for quarks and leptons, Ω_i signifies the potential for species i and B is the

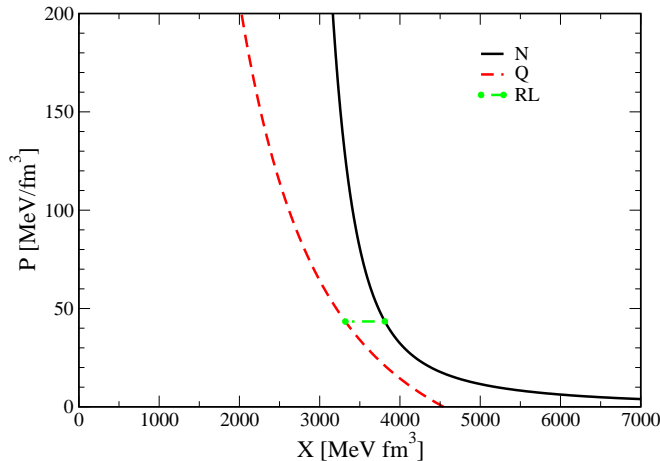


FIG. 3. (Color online) The Poisson's adiabats plotted in the $X - P$ plane both for NM and QM. Dash-dotted line (RL) indicate baryon density and energy density jumps for the equilibrium PT.

bag constant. The second term is for the interaction of quarks. μ is the baryon chemical potential and a_4 is the quark interaction parameter, varied between 1 (no interaction) and 0 (full interaction). We have only three quark species the u, d and s quarks. The masses of the u and d quarks are 5 and 10 MeV respectively and the mass of s quark is taken to be 100 MeV. We choose the values of $B^{1/4} = 140$ MeV and $a_4 = 0.5$. We choose such parameter setting because we wanted to have PT happening beyond the saturation density. With the given EoSs we plot the star sequences (M-R curves) shown in fig. 1a and mass-energy density curves in fig 1b. It is easy to observe that that the NL3 model generates quite massive stars, the maximum being $2.8 M_\odot$ with radius about 13 km. The sequence for the Qs generates less massive stars but still satisfies the present bound. Such stars are composed entirely of QM and are not entirely stable against NM. Therefore, a pure QS may not be absolutely stable and its outer region may convert into NM. Such conditions can give rise to stars which have a quark core surrounded by hadronic outer layers known as hybrid stars (HS).

The equilibrium PT point between the two phases can be calculated by plotting the pressure of the two phases as a function of chemical potential (fig 2). The point of crossing of the two curves gives the PT point. Below the crossing point the matter is hadronic and above it is quark (as shown in fig 2). The PT is implemented assuming Maxwell's construction. The TOV equations are solved to obtain the star sequence of the hybrid stars

(curve c of fig 1a). The low mass stars are all pure hadronic and the two curve overlap as the central density in these stars are not high enough to have PT. However, once the stars central density crosses the threshold value, QM stars to appear in their core and we obtain a separate branch, as the mass and radius both differs from the NSs.

The EoS and the equilibrium PT can also be represented in the form of poisons adaibats as shown in fig 3. The pressure is plotted as function of parameter X given by $X \equiv (\epsilon + p)/n_b^2$. The straight horizontal line connecting the two phases represents equilibrium PT. As we go towards the star core the pressure increases whereas the value of X decreases. The X value of NM is larger than that of QM because for the same value of pressure the density of QM is higher. During the PT there is a jump in the value of X , which becomes stronger at large densities. The equilibrium PT is difficult in old cold pulsars unless there is some sudden fluctuation in the thermodynamic quantities which can grow to give a step like feature. We assume such step like discontinuity generated near the star center and which propagates outwards bringing about a PT. The PT front burns the HM and leaves behind a compressed quark core. At relatively low density region the discontinuity diminishes and PT fronts stops. It is also assumed that the discontinuity happens only in a very thin layer in comparison to the star radius.

III. MAGNETIC FIELD ON THE STAR STRUCTURE

In the present work our main aim is to study the effect of strong magnetic fields in the PT of compact stars. Such strong magnetic field would also invoke significant mass modification and structural change in compact stars. The details of the calculation can be found in our previous paper [44]. Here we only mention the basic details and study their effect on the given stars sequences. The deformation of the star mainly arises due to non-uniform magnetic pressure in different direction. In the rest frame of the fluid, the magnetic field is in the z-direction, the energy density and pressure are given by

$$\varepsilon = \varepsilon_m + \frac{B^2}{8\pi} \quad (3)$$

$$P_{\perp} = P_m + \frac{B^2}{8\pi} \quad (4)$$

$$P_{\parallel} = P_m - \frac{B^2}{8\pi}. \quad (5)$$

where ε is the total energy density, ε_m is the matter energy density and $\frac{B^2}{8\pi}$ is the magnetic stress. P_\perp and P_\parallel are the perpendicular and parallel components of the total pressure with respect to the magnetic field. P_m is the matter pressure.

The total pressure in both the direction can be written in a single equation in terms of spherical harmonics

$$P = P_m + [p_0 + p_2 P_2(\cos\theta)]. \quad (6)$$

$p_0 = \frac{B^2}{3.8\pi}$ is the monopole contribution and $p_2 = -\frac{4B^2}{3.8\pi}$ the quadrupole contribution of the magnetic pressure.

Similarly the metric describing a axially symmetric star can formulated as a multipole expansion

$$ds^2 = -e^{\nu(r)}[1 + 2(h_0(r) + h_2(r)P_2(\cos\theta))]dt^2 \quad (7)$$

$$+ e^{\lambda(r)}[1 + \frac{e^{\lambda(r)}}{r}(m_0(r) + m_2(r)P_2(\cos\theta))]dr^2 \quad (8)$$

$$+ r^2[1 + 2k_2(r)P_2(\cos\theta)](d\theta^2 + \sin^2\theta d\phi^2), \quad (9)$$

where h_0, h_2, m_0, m_2, k_2 are the corrections up to second order.

The Einstein field equations can be solved to find the metric potentials in terms of perturbed pressure and hence can be solved to calculate the mass modification and axial deformation.

To solve the Einstein equation we need to describe the magnetic field inside the star. In our calculation we use a simple phenomenological density dependent magnetic field profile given by [44–46], and is parametrized as

$$B(n_b) = B_s + B_0 \left\{ 1 - e^{-\alpha \left(\frac{n_b}{n_0} \right)^\gamma} \right\}. \quad (10)$$

where, B_s is the surface magnetic field and B_0 is central field. The surface field is assumed to be 10^{15} G and central field is 10^{18} . We assume $\alpha = 0.01$ and $\gamma = 2$, which is quite a gentle variation of the magnetic field inside the star.

Using the given prescription we calculate the effective stars sequence for the three generations of stars (NS, QS and HS). In fig 1 we find that such strong magnetic fields significantly changes the mass and radius of the stars. The masses of the stars increases and they also take the shape of oblate spheroid, differing in the equatorial and polar directions.

IV. FLUID DYNAMIC CONSERVATION CONDITIONS

The differential form of energy-momentum conservation law for a fluid dynamical system is given by

$$D_\mu T^{\mu\nu} = 0 \quad (11)$$

where,

$$T^{\mu\nu} = w u^\mu u^\nu - p g^{\mu\nu}. \quad (12)$$

w is the enthalpy ($w = \epsilon + p$), $u^\mu = (\gamma, \gamma v)$ is the normalized 4-velocity of the fluid and γ is the Lorentz factor. $g^{\mu\nu}$ is the metric tensor chosen as $(1, -1, -1, -1)$ using standard flat space-time convention. Along with this the baryon number is also conserved for an isolated system such as CSs. The conservation laws can also be realized in the form of discontinuous hydrodynamical flow usually in shock waves. We assume that the PT happens as the single discontinuity fronts propagates separating the two phases, therefore we denote “ h ” as the initial state ahead of the shock (NM) front and “ q ” as the final state behind the shock (QM).

Across the front the two phases are related via the energy-momentum and baryon number conservation. The relativistic conservation conditions for the space-like (SL) and time-like (TL) shocks are derived from the above generalized equations [37, 38, 47].

a. Space-like

$$w_h \gamma_h^2 v_h = w_q \gamma_q^2 v_q, \quad (13)$$

$$w_h \gamma_h^2 v_h^2 + p_h = w_q \gamma_q^2 v_q^2 + p_q, \quad (14)$$

$$n_h v_h \gamma_h = n_q v_q \gamma_q \quad (15)$$

b. Time-like

$$w_h \gamma_h^2 - p_h = w_q \gamma_q^2 - p_q, \quad (16)$$

$$w_h \gamma_h^2 v_h = w_q \gamma_q^2 v_q, \quad (17)$$

$$n_h \gamma_h = n_q \gamma_q \quad (18)$$

However, when strong magnetic fields are present, the conservation condition gets modified. It now has both matter and magnetic contributions [37]. Assuming an ideally infinitely conducting fluid, the electric field vanishes. Also the conservation are solved in a special frame called HT frame (HT) [48] where the fluid flows along the magnetic lines and there

are no $\vec{u} \times \vec{B}$ electric fields. In this frame the magnetic field and the matter velocities are aligned. We assume that x -direction is the normal to the shock plane. The magnetic field is constant and lies in the $x - y$ plane. Therefore the velocities and the magnetic fields are given by v_x and v_y and by B_x and B_y respectively. The angle between the magnetic field and the shock normal in the HT frame is denoted by θ .

Therefore the conservation conditions now reads as

a. Space-like

$$w_h \gamma_h^2 v_{hx} = w_q \gamma_q^2 v_{qx}, \quad (19)$$

$$w_h \gamma_h^2 v_{hx}^2 + p_h + \frac{B_{hy}^2}{8\pi} = w_q \gamma_q^2 v_{qx}^2 + p_q + \frac{B_{qy}^2}{8\pi}, \quad (20)$$

$$w_h \gamma_h^2 v_{hx} v_{hy} - \frac{B_{hx} B_{hy}}{4\pi} = w_q \gamma_q^2 v_{qx} v_{qy} - \frac{B_{qx} B_{qy}}{4\pi}, \quad (21)$$

$$n_h v_{hx} \gamma_h = n_q v_{qx} \gamma_q. \quad (22)$$

b. Time-like

$$w_h \gamma_h^2 - p_h + \frac{B_{hy}^2}{8\pi} = w_q \gamma_q^2 - p_q + \frac{B_{qy}^2}{8\pi}, \quad (23)$$

$$w_h \gamma_h^2 v_{hx} = w_q \gamma_q^2 v_{qx}, \quad (24)$$

$$w_h \gamma_h^2 v_{hy} = w_q \gamma_q^2 v_{qy}, \quad (25)$$

$$n_h \gamma_h = n_q \gamma_q. \quad (26)$$

For the HT frame we also have

$$\frac{v_{hy}}{v_{hx}} = \frac{B_{hy}}{B_{hx}} \equiv \tan \theta \quad (27)$$

$$\frac{v_{qy}}{v_{qx}} = \frac{B_{qy}}{B_{qx}} \equiv \tan \theta_r. \quad (28)$$

The assumption of infinite conductivity gives the electric field to be zero. The Maxwell equation of no monopoles $\nabla \cdot \vec{B} = 0$ gives

$$B_{hx} = B_{qx}. \quad (29)$$

The TL conservation conditions leads to some interesting results in HT frame. Dividing eqn. 2 by eqn. 3, we get

$$\frac{v_{hy}}{v_{hx}} = \frac{v_{qy}}{v_{qx}}. \quad (30)$$

Combining this with eqn. 5 and eqn. 6, we have

$$\frac{B_{hy}}{B_{hx}} = \frac{B_{qy}}{B_{qx}}. \quad (31)$$

But eqn. 7 says $B_{hx} = B_{qx}$, therefore we have $B_{hy} = B_{qy}$.

Therefore eqn. 1 now becomes

$$w_h \gamma_h^2 - p_h = w_q \gamma_q^2 - p_q \quad (32)$$

Same as the non magnetic case.

Eqn. 2 and 3 can be combined in a single equation

$$w_h \gamma_h^2 v_h = w_q \gamma_q^2 v_q \quad (33)$$

Therefore, the TL conservation equation remains the same as non magnetic case. The magnetic field has no effect on the TL PT or discontinuity. This is an interesting outcome.

V. RESULTS

A. SL shocks

Fluctuation of the thermodynamic quantities at the center of the star starts the PT. Let us first examine all the features of a space-like shock which is common in astrophysical environment. Later we will discuss about the TL shock. The PT would depend on the process being exothermic or endothermic. At the center of the star first there is a deconfinement transition and then there is conversion to stable QM. At a certain point as the matter converts from NM to QM there is sharp change in the thermodynamic variables (like density, pressure etc). The propagation of the PT front depends on the energy difference between the NM and QM. If the energy of the NS is greater than that of the QS then the conversion is exothermic and shock like features can develop. However, the energy difference depends on the EoS of NM and QM, the baryon density at which the PT is taking place and also on the velocity of the shock front. The above conservation conditions are written in the rest frame of the conversion front. We solve our problem in this frame and go the global frame where QM is at rest. In our calculation, for the front rest frame, NM velocity is represented as v_h and QM velocity as v_q . In the global frame, NM velocity is given by v_n

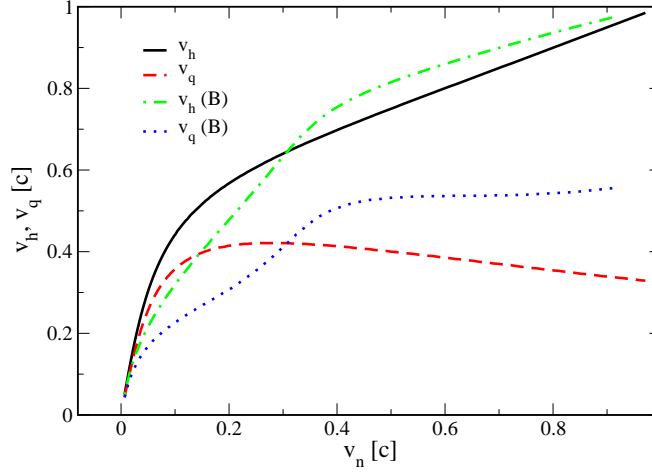


FIG. 4. (Color online) The variation of v_h and v_q as a function of v_n is shown. a) Solid (without B) and dashed (with B) curve corresponds to v_h and dotted (without B) and dash-dotted (with B) curve corresponds to v_q . Curves are shown for $\alpha = 2\alpha_0$.

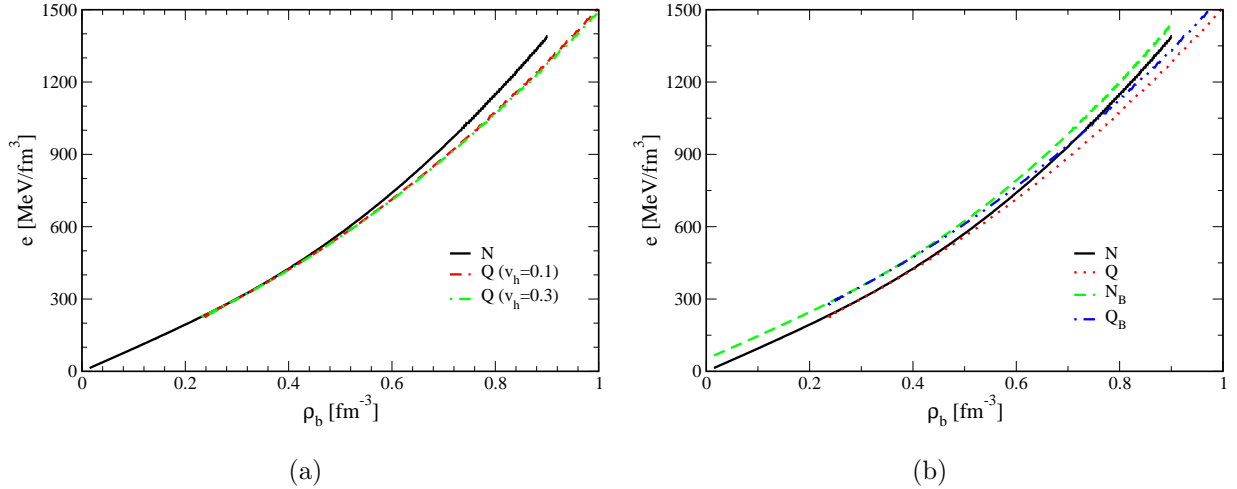


FIG. 5. (Color online) The energy density of the NP and QP as a function of baryon density is shown. a) Curves without magnetic field contribution, plotted for two given values of v_h , 0.1 and 0.3. b) Curves with contribution from matter and magnetic field are shown with $v_h = 0.3$.

and front velocity as v_f . In this global frame the NM moves toward the center with velocity $v_n = (v_h - v_q)/(1 - v_h v_q)$. The front velocity near the center can assumed to be $v_f = -v_q$, where v_h and v_q are the quantities in the HT frame.

In this calculation we would see the evolution of our relevant parameters in terms of v_n and hadronic density ρ_b . For such analysis first we have to know how v_h and v_f varies with

v_n . This is shown in fig 4. We see that initially as v_n increases from 0 to 0.1 there is a sharp rise in v_h from 0 to 0.5 after which the slope of v_h decreases and it gradually goes to 1 as v_n reaches 1. However, the value of v_h is always greater than v_n . The difference is high at low values of velocity and decreases as velocity increases. In other words we can say that initially as v_h increases, the value of v_n does not change much and only after v_h goes beyond 0.5 that the value of v_n increases rapidly to match the value of v_h as they both goes to 1. On the other hand if we see the variation of v_f (which is same as v_q only the direction changes) we find that initially v_f rises rapidly to attain a maximum value of 0.42 at $v_n = 0.2$ and from there it decreases slowly to attain value $1/3$ as both v_n and v_f goes to 1. Near the center of the star the velocity of the incoming matter is largest. As the shock wave propagates outwards from the center, the incoming matter velocity decreases but the front velocity increases gradually. However, after v_n becomes less than 0.2, the front velocity drops rather quickly and vanishes at $v_n \rightarrow 0$. It is interesting to note that the conservation conditions act in such a way that even without any dissipation mechanism there is some type of deceleration which drives the front velocity to zero at some point inside the star, corresponding to an equilibrium configuration with the static phase boundary.

With our choice of EoS of NM and QM, the equilibrium PT occurs around 2 times nuclear saturation density ρ_s . If there is sudden fluctuation of matter at such high density then the PT is no longer an equilibrium PT. Such delayed PT can occur at higher densities and can be a violent one. Such PT would depend primarily on the energy difference between hadronic state and the shocked quark state. In fig 5a we see that the energy of the NM is greater than the energy of the QM (corresponding to a particular density) and therefore the PT is an exothermic one, and shock like features can develop. We also see that the QM does not go to very low densities because as the PT occurs the burned matter is compressed, thereby increasing its density. We also find that at densities close to $2\rho_s$ the energy difference between the un-shocked and shocked matter becomes almost equal. Beyond these densities inside the star it is difficult for the matter to undergo PT. At such densities it is expected that the dynamical shock-front would decelerate and ultimately stop. However, such analysis can only be done once we do the full dynamic calculation, which is beyond the scope of this article. We have shown curves for two different incoming hadronic velocities (v_h) and the behavior of the curves does not change much. In fig. 5b we show similar curves but with contribution from magnetic energy. The magnetic energy adds to the matter energies and

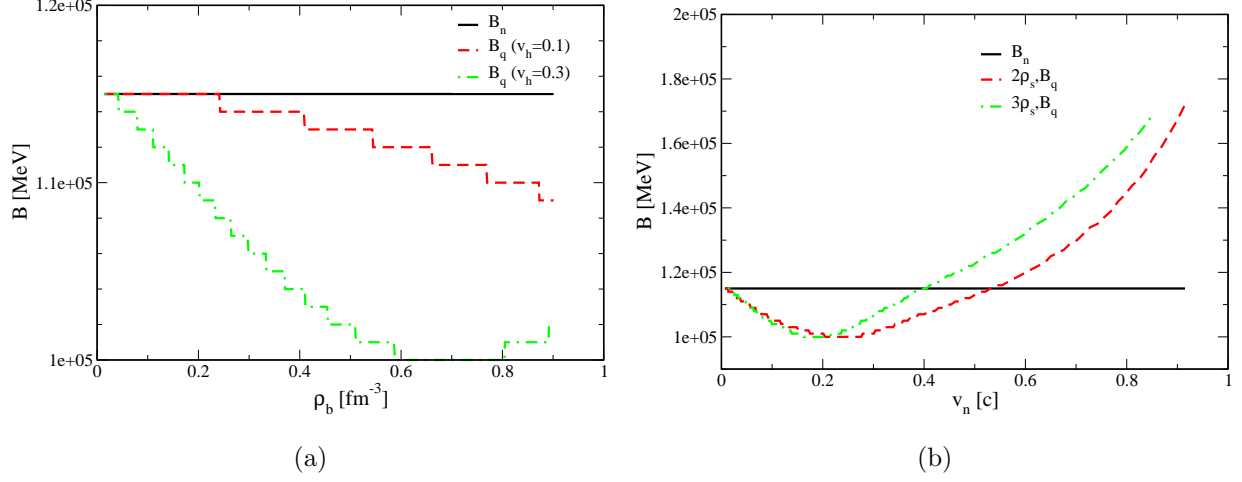


FIG. 6. (Color online) Magnetic field in the NP and QP are shown as a function of ρ_b and v_n . a) Solid line is for NP and the dashed and dash-dotted lines are for QP with $v_h = 0.1$ and $v_h = 0.3$ respectively. b) Similar set of curves are plotted as a function of v_n for two different ρ_b . Quantities with subscript n corresponds to NP and with subscript q corresponds to QP.

makes the curves stiffer, however the PT is still exothermic.

We calculate the strength of magnetic field in the QM after the front has passed. We want to know whether the resultant star would become more or less magnetic due to the burning process. We have studies the magneto hydrodynamic conservation equations for magnetic field of strength 10^{18} G and angle $\theta = 30^\circ$. If the magnetic field is perpendicular to the shock front then there is no effect as then we would only have x -component of magnetic field. From Maxwell's equation, they are equal in the burned and unburnt matter (eqn 29). The change in the total magnetic field is only due to the difference in the magnetic field in the y -direction. It is usually assumed that if the surface magnetic field is of the order of 10^{15} G then the central magnetic field can be of the order of few times 10^{18} G (from Virial theorem). Therefore we have kept our magnetic field to be of the order of 10^5 MeV which is equal to 1.414×10^{18} G. In usual pulsars the magnetic axis is slightly tiled from the body axis. However, the tilt is not very large. It can be safely assumed that the tilt is within 30° . If the PT front starts from the center and we consider our star to almost spherical and of uniformly varying density then the PT front would also be spherical. If this is so then the magnetic field can be at most be at an angle 30° to the PT front. Keeping this in mind we have kept our θ to be 30° .

In fig 6 we plot the initial and final magnetic field as a function of both density and

v_n . As can be seen from fig 6a the magnetic field in the burned matter is smaller than the magnetic field in the QM. As the density increases the magnetic field in the burned matter becomes much smaller. However, the change in magnetic field across the two sides is less than 1%. This small change in the magnetic field may be due to fact that the magnetic field which arrives in eqn. 21 of the conservation equations acts in the opposite direction of the matter contribution. It somehow opposes the PT. Therefore some amount of magnetic energy is spent in continuing the PT process. Therefore, the magnetic field in the QM is slightly smaller. As the velocity of the incoming matter increases the magnetic field in the QM decreases much further.

Next we plot the magnetic field on two sides as a function of v_c in fig 6b. We see that initially at smaller values of v_c the magnetic field decreases and attains a minimum value at around $v_n = 0.2$ (corresponding to $v_h = 0.48$). From thereon the magnetic field increases and at values greater than $v_n = 0.53$ ($v_h = 0.83$) the magnetic field in the QM becomes greater than that of NM (there is a crossing in the curves). The nature of the curves remains the same for $\rho_b = 3\rho_s$, only the crossover occur at much smaller velocities for such density. Such nature may be due to the fact that at such v_n the value of v_h becomes quite high and then the conservation condition is driven mostly by the matter enthalpy and pressure term than that of magnetic term.

The reflected angle θ_r changes both with ρ_b and v_n . The incident angle θ is always fixed at 30° for star with magnetic field. In fig 7a, we plot the reflected angle as a function of ρ_b for two incoming matter velocity v_h . If v_h is small (0.1) then at smaller densities the reflected angle is also close to 30° but as the density increases reflected angle decreases and goes to about 23° . The negative sign in the reflected angle means that the reflected matter velocities and magnetic field are above the plane perpendicular to the shock front (the x-axis). For higher value of $v_h = 0.3$, for lower densities the reflected angle is still close to 30° but as the density increases the reflected angle decreases very fast and at about $\rho_b = 0.7$ it crosses the x-axis and goes to positive values. So there is complete change in angular directions at higher densities. This means, instead of pointing upwards the matter velocities and magnetic fields points downward in the burned matter. In fig 7b we plot θ_r as a function of v_n . We have plotted the curves for two different densities ($2\rho_s$ and $3\rho_s$). We find that as the velocity increases θ_r decreases and becomes zero at $v_n = 0.24$ ($v_h = 0.54$). Thereafter it increases in the positive direction and goes to about 60° at higher velocities. The outflow

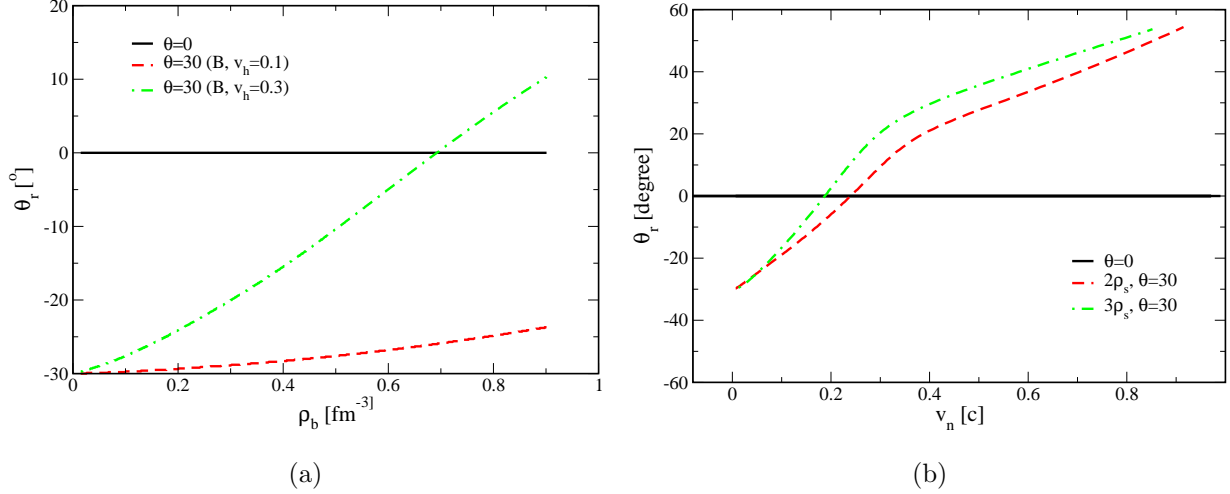


FIG. 7. (Color online) Reflected angle (θ_r) is plotted as a function of ρ_b and v_n . a) Solid line is for non-magnetic star (no angular dependence) and the dashed and dash-dotted lines are for magnetic star with $v_h = 0.1$ and $v_h = 0.3$ respectively. b) Similar set of curves are plotted as a function of v_n for two different ρ_b .

velocity and magnetic field in the burned QM changes direction at higher velocities. The curve for $\rho_b = 3\rho_s$ shows almost similar pattern only differing numerically.

The variation of matter velocities and comparing them is an important tool to understand whether a shock propagation is a detonation or deflagration. If the velocity of the burned matter is greater than unburnt matter, the PT is a detonation one, whereas if the velocity of unburnt matter is greater than burned matter it is a deflagration. Detonation is very fast burning whereas deflagration is slow combustion. Another way of determining detonation and deflagration is comparing their energy and pressure. It can be classified as

- a) $v_q > v_h$, $e_q - p_q < e_h - p_h$ detonation.
- b) $v_q < v_h$, $e_q - p_q > e_h - p_h$ deflagration.

In fig 8a we plot v_h and v_q as a function of ρ_b . We have compared it for two values of v_h , 0.1 and 0.3. We find that for all cases the value of v_q is smaller than v_h , signaling the PT would be a deflagration process. For $v_h = 0.1$, initially v_q rises very steadily with density and reaches its maximum value (0.086) around $2\rho_s$ which is close to the equilibrium PT density. After that it falls very slowly and takes a constant value at large densities. For the magnetic case v_q is slightly smaller than the non magnetic one but the nature of the curve remains same. For $v_h = 0.3$, the rise of v_q is much faster but the maximum value (0.255) is achieved at the same density ($2\rho_s$). In this case the magnetic curve lies much lower than

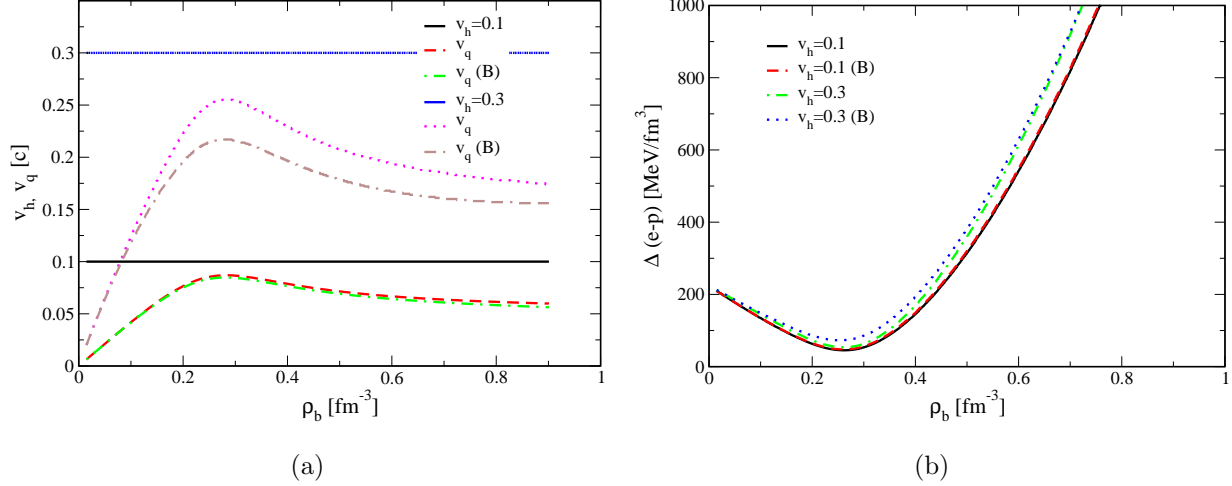


FIG. 8. (Color online) a) Curves in this figure drawn to compare v_h and v_q as a function of ρ_b . Solid curve shows $v_h = 0.1$ and the two curves below it shows the corresponding v_q with (dashed) and without (dotted) magnetic effect. The other three family is for $v_h = 0.3$ and its corresponding v_q . b) The difference of $(e-p)$ for the QP and NP ($\Delta(e-p)$) is shown as a function of ρ_b . The solid (without magnetic effect) and the dotted (with magnetic effect) are plotted for $v_h = 0.1$ and the dashed and dash-dotted curves are for $v_h = 0.3$.

the non magnetic one and the maximum value of v_q is 0.216.

Following the condition given for determining detonation and deflagration we plot $(e_q - p_q) - (e_h - p_h)$ (denoted as $\Delta(e-p)$ in the fig 8b) as a function of ρ_b . The value is always positive, establishing the claim that the PT is of deflagration type. At lower densities the value is small and it increases with density, meaning that the deflagration speeds up at higher densities. For $v_h = 0.1$, the magnetic and non-magnetic curve almost overlap, whereas for $v_h = 0.3$ the magnetic curve lies below the non magnetic curve. The nature of the curves remains same for all.

The value of v_n depends both on v_h and v_q . Although v_h is kept constant for our calculation v_n changes with ρ_b as the value of v_q changes. Therefore, it is interesting to see how the front velocity v_f and v_n changes with ρ_b . In fig 9 we have plotted the v_n and v_f as a function of ρ_b . At low densities v_n first decreases and attains a minimum value at $2\rho_s$. Beyond this point v_n gradually increases and attains a constant value at higher densities. The nature of v_f is completely opposite, it first increases at low densities and attains a maximum value at $2\rho_b$ and then gradually decreases to attain almost a constant value at higher densities. In the region of our interest ($\rho_b > 2\rho_s$) v_f is always greater than v_n . The nature of both v_n

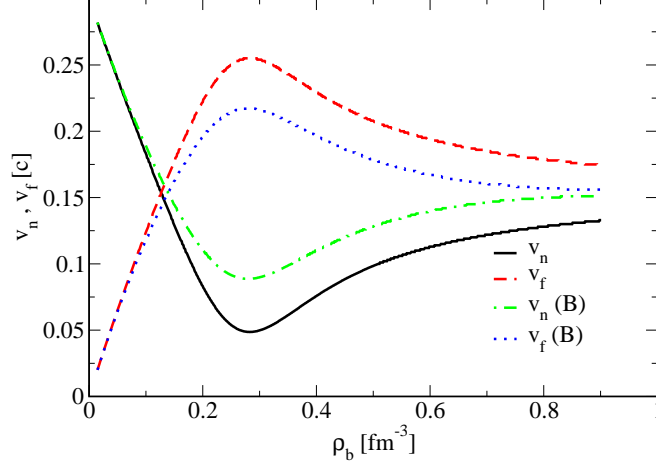


FIG. 9. (Color online) The incoming matter velocity v_n and the front velocity v_f in the global frame (QM rest frame) are shown as a function of ρ_b . The solid and the dot-dashed lines are for v_n without and with magnetic effect and the dashed and dotted lines are for corresponding v_f . Curves are plotted for

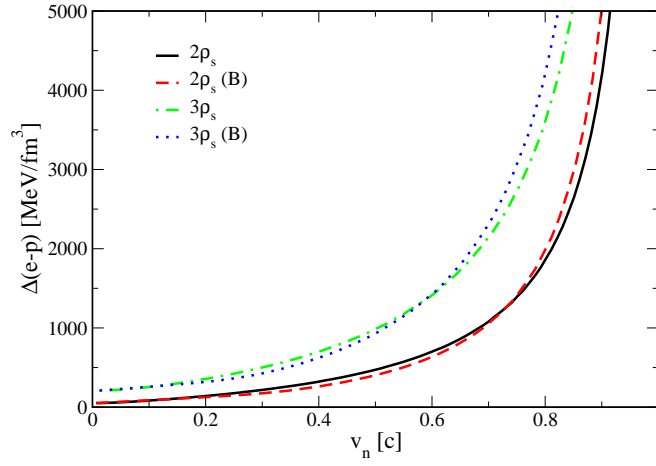


FIG. 10. (Color online) The difference of $(e - p)$ for QP and NP is plotted as a function of v_n . The solid (without magnetic effect) and the dashed (with magnetic effect) are plotted for $\rho_b = 2\rho_s$ and the dot-dashed and dotted curves are for $\rho_b = 3\rho_s$

and v_f are same for a magnetic star only their corresponding values are smaller than the non magnetic star. Therefore, the difference between the values of v_n and v_f when they become almost constant at high densities is smaller (they almost becomes same) than the non magnetic case.

Next we check the variation of $\Delta(e - p)$ with v_n in fig 10. The value is always positive

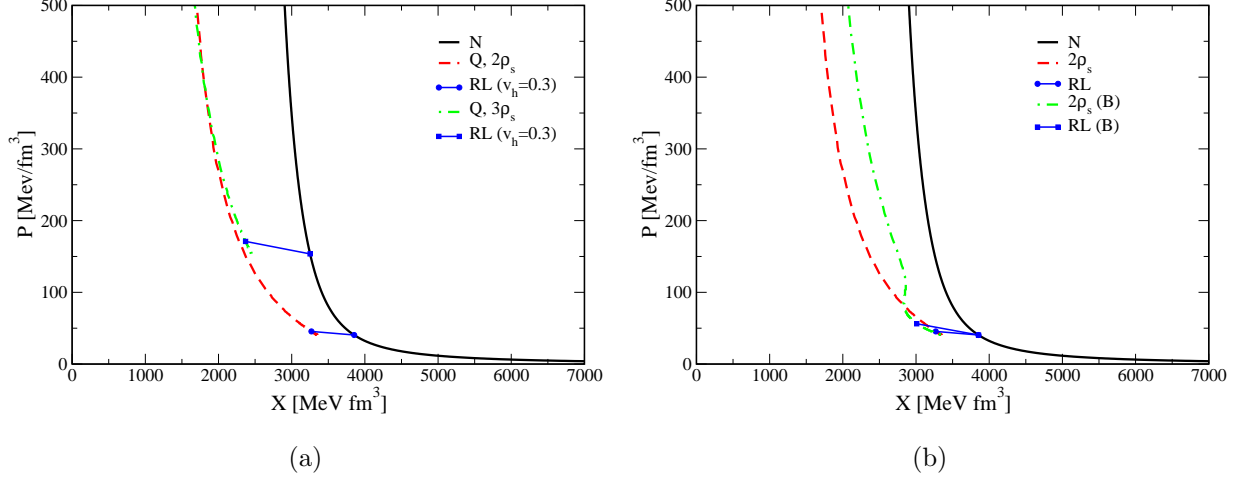


FIG. 11. (Color online) TA shown in the $X - P$ plane. a) Curves plotted to show the jump from NM to QM happening at two densities $\rho_b = 2\rho_s$ (dashed line) and $3\rho_s$ (dash-dotted line). The lines connected with dots and cross are the so called RL, showing PT from NM to QM for $v_h = 0.3$. b) TA for magnetic (dash-dotted line) and non-magnetic stars (dashed line). The RL is drawn for $v_h=0.3$ and $\rho_b = 2\rho_s$. The zero-temperature isotherm of NM is shown by the solid line. The quark shocked adiabat curves are obtained by varying v_h from 0 – 1.

implying the burning process to be a deflagration one. As the velocity increases the value increases implying a strong deflagration. At very high densities the value is so large that we can infer that in any star the starting burning process is always a deflagration one. There is slight change in the curves for magnetic and non magnetic one, implying that even for magnetars the starting burning mechanism is always slow burning.

Nuclear to quark PT can also be realized if we plot the taub adiabat (TA) curves. TA is a single equation which can be obtained from the conservation equations and reads as

$$(p_n + \varepsilon_q)X_q = (p_q + \varepsilon_n)X_n, \quad (34)$$

where $X_i = w_i/n_i^2$. The thermodynamic quantities of a given phase can be regarded as a function of this X . For a given initial state of NM (a fixed point in the curve) one can have a TA of the QM by a line in the $X_q - p_q$ plane. The slope of the so called "Rayleigh" line, connecting this initial point in the NM with the point (X_q, p_q) on the TA is related to the incoming velocity v_h . As v_h increases the slope of the line increases as $(\gamma_h v_h)^2$ [49]. Therefore, for each v_h there is a specific point on the TA corresponding to state of compressed QP. In fig 11 we have plotted such TA. The black line represents the initial NM EoS plotted in this

plane. Assuming that the PT happens at $2\rho_s$, when the incoming matter velocity is 0.3 (in units of c), we get a definite point in the shocked QM TA curve. The blue line represents the Rayleigh line (RL). The whole adiabat is obtained by varying v_h from 0 to 1. For a given ρ_b we get one such curve for shocked matter in the $X - p$ plane. However, when the PT takes place at $3\rho_s$ for the same v_h we get some different point as shown in the figure. Connecting points for different v_h we get a different curve. As the PT occurs at higher density the TA curve starts from some higher point in the $X - p$ plane.

In fig 11b we have plotted p as a function of X taking into account the effect of magnetic field, however it is not exactly a TA as it does not satisfies eqn. 34 due to extra magnetic terms. The curve for the magnetic star shows an interesting feature. The incident angle of the velocity and the magnetic field is important in determining the nature of the outgoing matter. As can be seen from the figure initially the magnetic curve lies below the non magnetic curve, however beyond a certain v_h the two curve crosses and beyond that velocity the magnetic curve lies above the non magnetic curve. The interesting nature of magnetic field and the θ_r variation with v_n as discussed previously is responsible for such a variation. The crossover takes place at $v_h = 0.54$ (corresponding to $v_n = 0.24$) same as the crossover point for magnetic field and θ_r . This implies that if the PT happens for magnetic stars initiated by such high value of v_h the resultant burned star is less compressed than usual non magnetic stars.

We can plot same TA curve by varying ρ_b for some fixed v_h . In fig 12 we plot it TA like curves for $v_h = 0.3$, both with and without magnetic field. The magnetic field pushes the curve towards lesser X , thereby signifying that the PT is now making the QM more compressed. There is no crossover in these curves as the magnetic and θ_r variation with ρ_b is simple. The slope of the RL for the magnetic curve is softer than the non magnetic curve.

The dynamics of the star transformation depends strongly of the ratio of densities before and after the PT, which is usually represented as $\lambda = b_q/b_h$. It is the ratio of quark density to hadron density. If this quantity exceeds the ratio $3/2$ then the matter in the vicinity of the phase boundary becomes unstable and readily converts to a new phase (QM). We plot λ as a function of densities in fig 13a. For $v_h = 0.3$ we see that at lower densities the value is smaller than $3/2$ and therefore for these densities it is difficult for PT to occur even on sudden density/pressure fluctuation. However as the density rises λ also rises and beyond $\rho_b = 0.5 \text{ fm}^{-3}$ λ crosses the $3/2$ value. Therefore if the central densities of a star is above

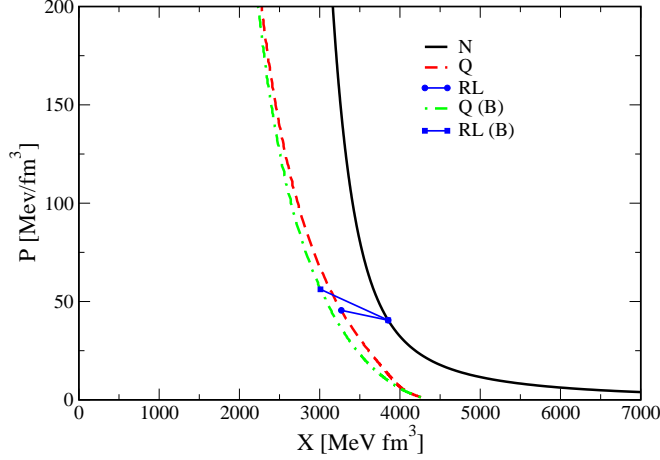


FIG. 12. (Color online) TA obtained by varying ρ_b for fixed $v_h = 0.3$. The dashed curve is for non-magnetic star and the dash-dotted curve is for magnetic star. The RL are obtained for $\rho_b = 2\rho_s$.

$3\rho_s$ then for such stars it is quite possible that a small perturbation in density at the center can result in the initiation of the PT process. After the PT starts, the dynamics of the PT is then governed by the dynamical equations. We have plotted λ vs ρ_b for the magnetic stars as well. We find that it is slightly easier to start PT if the star is magnetic. The curve for $v_h = 0.1$ is similar, however, the difference in value of λ for magnetic and non magnetic star is negligible.

λ can also be plotted at a function of incoming matter velocity v_h for some fixed ρ_b . In fig 13b we have plotted the same for $\rho_b = 2\rho_s$. It is clear from the figure that at small v_n lambda is less than $3/2$. Therefore, to have shock induced PT at such densities v_n needs to be high. From the figure we see than for v_n greater than 0.2 ($v_h > 0.5$) shock like PT can be induced. Beyond, this value λ increases steadily and beyond 5 – 6 times ρ_s the value of λ increases very fast. Stars having such high central densities are very prone to such violent shock induced PT. In the figure we also plot λ for magnetic stars. We find that magnetic stars are less prone to PT than non-magnetic stars. Initially, at low velocities both the curve overlap, however, as velocity increases the magnetic curve goes slightly below the non magnetic curve. Although, at higher velocities they again cross the non magnetic curve and becomes much stiffer.

The main cause of the front propagation is due to the energy and pressure discontinuity

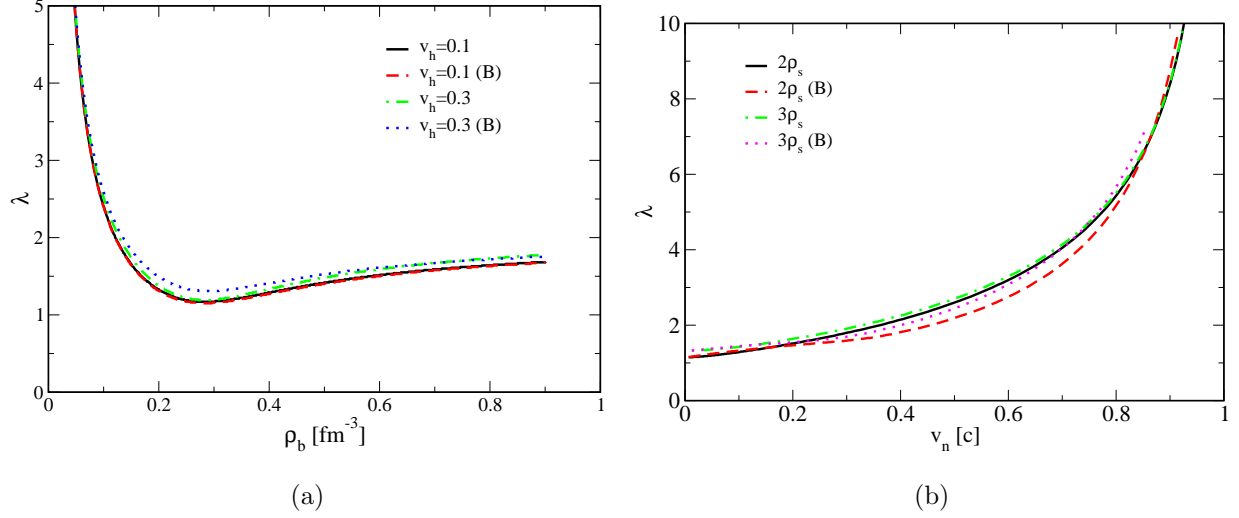


FIG. 13. (Color online) The ratio of density of QM and NM (denoted as λ) at the phase boundary as a function of ρ_b and v_n is shown. a) λ for non-magnetic (solid and dot-dashed line) and magnetic (dashed and dotted line) are compared for two values of v_h . b) λ for non-magnetic (solid and dot-dashed line) and magnetic (dashed and dotted line) are compared for two values of ρ_b .

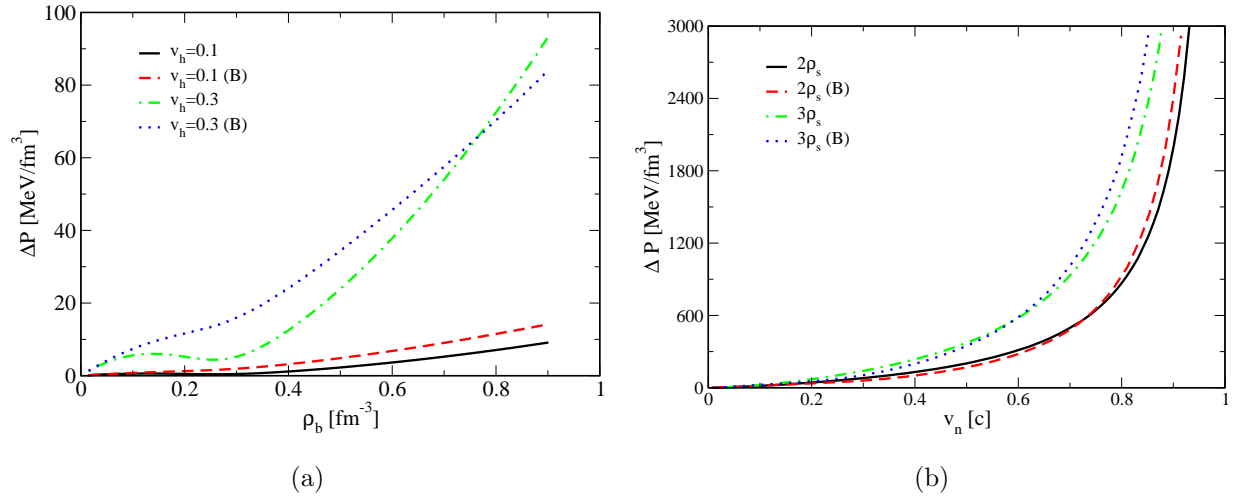


FIG. 14. (Color online) Difference between the pressure in the QP and NP (ΔP) as a function of ρ_b and v_n are drawn. Curve nomenclature are same as the above figure. A) curves are plotted for two different v_h , 0.1 and 0.3. b) Curves are plotted for two ρ_b , $2\rho_s$ and $3\rho_s$.

at the phase boundary. The greater the discontinuity the more probable is the chances of shock propagation. In the rest frame of the front, if the pressure and density is higher on the left side (NM) than on the right (QM), the discontinuity would move towards the right. In the case of star the density and pressure of the burned QM is greater than that of unburned

NM, therefore the shock would propagate to the NM converting more and more NM to QM. In fig 14a we plot the pressure discontinuity ($\Delta P = P_q - P_h$) as a function of baryon density and in fig 14b we plot it as a function of v_n . From fig 14a it is clear that the pressure discontinuity is higher at high densities and decreases as we go to the lower densities. The discontinuity becomes lowest at the point where equilibrium PT would occur. For magnetic stars the pressure difference ΔP becomes greater than the previous case. As we go to higher densities the difference between the two decreases, and the two curve cross each other at around $5\rho_s$. Therefore, at low densities it is easier to form shock like discontinuity for a magnetic star, however, when the central density of stars is greater than 5 times ρ_s then it is easier for non magnetic stars to induce shock like PT. In fig 14b, we have plotted ΔP as a function of v_c . We find that as v_c increases the pressure difference increases and increases asymptotically at velocities close to 1. Therefore, if the velocity of the incoming matter is very high shock induced PT is much easier to form and small fluctuation gives rise to strong shocks.

B. TL shocks

We have seen from our calculation that the magnetic field have no effect on TL shock if we assume infinite conductivity. All the conservation condition remains the same. Let us see here how the TL shock compares with the SL shock in the astrophysical scenario. The TL shock also satisfies the TA, and comparing it with SL shocks we find no such significant difference, only that it goes to much lower pressure values. At very low values of pressure, X increases with pressure and at around $X = 5600 \text{ MeV fm}^3$ there is turning of the curve and beyond that X decreases with pressure. The curve is shown in fig 15. However, at such low densities there may not be any PT and we can as well ignore it.

As can be seen from fig 16a, the value of λ is almost equal to one for all densities therefore it is difficult to start TL shock at star center. In fig 16b, we have plotted ΔP as a function of ρ_b and it shows negative values. That means pressure in the QP is lower than that of the hadronic phase and therefore the shock would not propagate to the right, converting NM to QM. It is true that for TL shocks the discontinuity in the thermodynamic quantities does not proceed as step like function, but instead the PT is via bubble like formation all across the matter. The bubble like formation can make the PT to take place instantly. However,

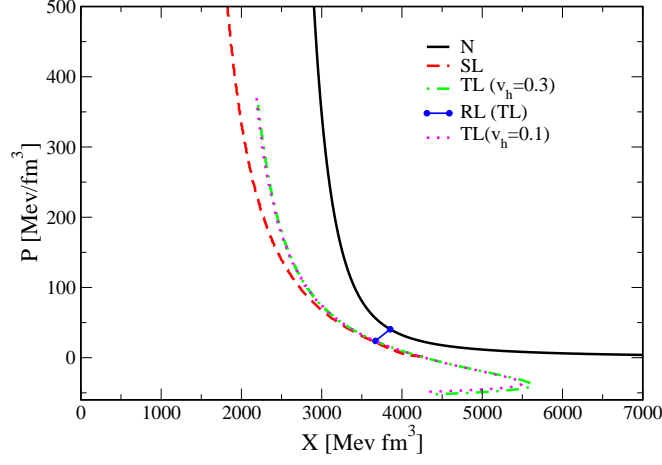


FIG. 15. (Color online) TA for TL PT. The solid line shows the isotherm of NM and the dashed line is the TA for SL shock transition. The dot-dashed and dotted curves are for TL shock transition for two different v_h , corresponds to 0.3 and 0.1 respectively. The RL is for $\rho_b = 2\rho_s$.

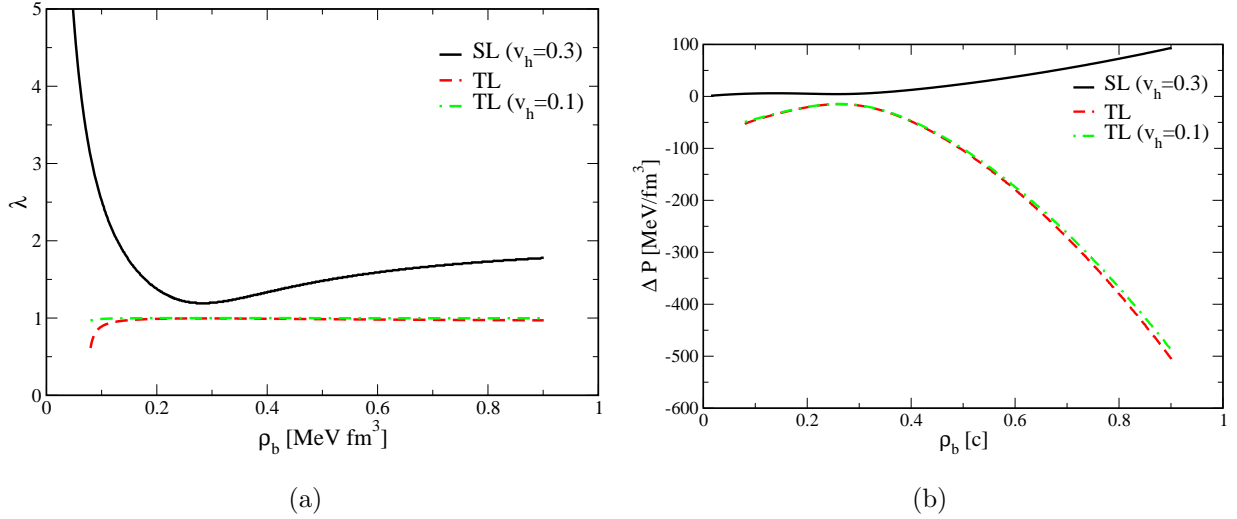


FIG. 16. (Color online) a) λ for TL shock transition is compared with SL shock transition. Solid line if for SL with $v_h = 0.3$ and dashed and dash-dotted lines are for TL with $v_h = 0.3$ and $v_h = 0.1$ respectively. b) Δp is shown with varying ρ_b , where the TL shock transition is compared with SL shocks. Curve labels are similar to (a).

such instances in astrophysical scenario is difficult to observe at cold high density matter.

VI. SUMMARY AND CONCLUSION

In this present article we mainly focus our attention to the effect of magnetic field on PT of a NS to QS. We have used relativistic MHS conservation condition to study this effect. For simplicity we have choose the HT frame (where the magnetic and matter velocities are aligned in the rest frame of the front) and we have also assumed infinite conductivity. Our aim is to categorize the PT process, whether it is a fast burning detonation or a slow combustion deflagration. Comparing the matter velocities and the energy-pressure of the respective phases we would be able to categorize the PT process. In our calculation we have use hadronic and quark EoS which are consistent with recent pulsar mass measurement. As a test case we have also examined what effect the strong magnetic field would have on the structure of the star. We have assumed magnetic fields of strength 10^{15} G at the surface of the star which are usually observed in magnetars. The central magnetic field is assumed to be of the order of 10^{18} G. Such magnetic fields are usually present at the cores of NS where the density is usually greater than 3 times saturation density ρ_s .

In our calculation we were studying the various quantities as a function of baryon density ρ_b . The baryon density which is relevant in our study is usually higher than 2 times ρ_s . On one hand, there is no equilibrium PT and so shock formation below such densities is difficult. On the other hand, Below this density such high magnetic field would make the matter very unstable and can give spurious results.

Initially, we have seen from the TA curves that shock like PT are much more stronger than equilibrium PT, and so it is more likely that a small fluctuation in the density and pressure at the star center would probably give rise to shock like discontinuity. Comparing the energies of the hadronic and QM as a function of baryon density we concluded that the process would be an exothermic one. Therefore, the PT induced by shock like discontinuity at the star center would propagate outwards, converting NM to QM. We have also studied the quark to hadronic density ratio at the phase boundary and found that even for small incoming velocity of NM the NM at the star core is unstable with respect to QM where the densities are greater than $3\rho_s$, and the NS would eventually convert to a QS. Similar, observation also came from comparing the pressure difference of the two phases.

Observing the criterion for the detonation and deflagration as described in the text and from the figures we found that the velocity of the NM is always greater than that of the

velocity of QM, which is the condition for a deflagration. Also the $(e - p)$ comparison of the respective phases comes to the same conclusion. The burning process at the star center starts always as a deflagration process. However, the actual burning process in the star as the PT front moves inside the star can only be obtained once we solve the dynamic process. In these calculation gravity does not appear, and as was shown by many authors [23] that presence of gravity can make the deflagration unstable. The instabilities can make the deflagration process convert to a detonation one.

It is also seen that at high densities and at high infalling matter velocities the magnetic angle changes sign. With respect to the star it can signify that the actual magnetic axis (MA) tilt of the star can change direction. Which can mean that a star with MA tilted to the right can undergo a PT and the resultant QS can have a MA tilted to the left. This can have huge effect on the observation of the pulsars. A pulsar which was previously recorded can undergo a PT and can completely disappear from us.

At small enough infalling matter velocities the resultant magnetic field of the QS is smaller than that of the NS. However, for higher value of infalling matter velocities the magnetic field of QM becomes larger. Although the magnetic field in the QM at smaller velocities is less than that of NM, this does not means that the QS is less magnetic than that of NS. The ultimate magnetic field of the QS after the PT is determined by many other factors, like the flux conservation. As the PT happens the QS contracts in size as it is more compact and asserting flux conservation of the magnetic field the magnetic field in the QS would rise. It may also depend on the temperature of the star and how much energy spend on the dynamic process. Therefore, it is wrong to assume from this discussion that the resultant QS is less magnetic.

The TL shock was found difficult to initiate in this astrophysical scenario in the PT of NSs. However, it may be because of the fact that we were only examining the case of step like discontinuity at the star center and had neglected bubble like PT scenario.

Although we have in detail discussed the magneto hydrostatic scenario of the PT of NS to QS, we have here only established the initial conditions and the possible PT mechanism. The actual dynamic of the PT would be complete once we study and understand the magneto hydrodynamic PT scenario solving the dynamic Euler's equations. Although such calculation would be very involved, it is on our immediate agenda.

ACKNOWLEDGMENTS

RM would like to thank SERB, Govt. of India for monetary support in the form of Ramanujan Fellowship and Early Career Research Award. RM and AS would like to thank IISER Bhopal for providing all the research and infrastructure facilities.

- [1] Weber, F., Pulsar as an astrophysical laboratory for nuclear and particle physics, (Institute of Physics Publishing, Bristol, 1999)
- [2] Glendenning, N. K., Compact Stars: Nuclear Physics, Particle Physics, and General Relativity, (Springer, New York, 2000)
- [3] Hewish A., Bell S. J., Pilkington J. D. H., Scott P. F. & Collins R. A., Nature 217, 709 (1968)
- [4] Gold T., Nature 218, 731 (1968)
- [5] Demorest, P., Pennucci, T., Ransom, S., Roberts, M., & Hessels, J., Nature, 467, 1081 (2010)
- [6] Antonidis, J., Freire, P. C. C., Wex, N. et. al., Science, 340, 448 (2013)
- [7] N. Itoh, Prog. Theor. Phys. 44, 291 (1970)
- [8] A. R. Bodmer, Phys. Rev. D 4, 1601 (1971)
- [9] Witten, E., PRD 30, 272 (1984)
- [10] N. K. Glendenning, Nucl. Phys. B Proc. Suppl. 24, 110 (1991), Phys. Rev. D 46, 1274 (1992)
- [11] C. Alcock, E. Farhi & A. Olinto, AstroPhys. J. 310, 261 (1986)
- [12] A. Drago, A. Lavagno & G. Pagliara, Eur. Phys. J. A 19, 197 (2004)
- [13] I. Bombaci & B. Datta, AstroPhys. J. 530, L69 (2000)
- [14] Z. Berezhiani, I. Bombaci, A. Drago, F. Frontera & A. Lavagno, AstroPhys. J. 586, 1250 (2003)
- [15] R. Mallick & P. K. Sahu, Nucl. Phys. A 921, 96 (2014)
- [16] A. Sedrakian, Astron. & Astrophys. 555, L10 (2013)
- [17] E. B. Abdikamalov, H. Dimmelmeier, L. Rezzolla & J. C. Miller, Mon. Not. R. Astron. Soc. 392, 52 (2009)
- [18] J. E. Horvath, Int. J. Mod. Phys. D 19, 523 (2010)
- [19] A. Drago, A. Lavagno & I. Parenti, Astrophys. J. 659, 1519 (2007)
- [20] A. Bhattacharyya, S. K. Ghosh, P. S. Joarder, R. Mallick & S. Raha, Phys. Rev. C 74, 065804

(2006)

- [21] L. M. Lin, K. S. Cheng, M. C. Chu & W. -M. Suen, *Astrophys. J.* 639, 382 (2006)
- [22] Olinto, A., *Phys. Lett. B*, 192, 71 (1987)
- [23] Horvath, J. E., & Benvenuto, O. G., *Phys. Lett. B*, 213, 516 (1988)
- [24] Cho, H. T., Ng, K. W., & Speliotopoulos, A. D., *Phys. Rev. Lett.*, 77, 1210 (1996)
- [25] Kulkarni, S. R., and Frail, D. A., *Nature* 365, 33 (1993)
- [26] Murakami, T., Tanaka, Y., Kulkarni, S. R., et al., *Nature* 368, 127 (1994)
- [27] Duncan, R. C., and Thompson, C., *AstroPhys. J.* 392, L9 (1992)
- [28] Thompson, C., and Duncan, R. C., *AstroPhys. J.* 408, 194 (1993)
- [29] Paczynski, B., *Acta. Astron.* 42, 145 (1992)
- [30] Melatos. A., *Astrophys J. Lett.* 519, L77 (1999)
- [31] Makishima, K., Enoto, T., Hiraga, J. S. & et al., *Phys. Rev. Lett.* 112, 171102 (2014)
- [32] S. Akiyama, J. C. Wheeler, D. L. Meier, & I. Lichtenstadt, *Astrophys. J.* 584, 954 (2003)
- [33] M. Obergaulinger, P. Cerd-Durn, E. Mller, and M. Aloy, *Astron. Astrophys.* 498, 241 (2009)
- [34] H. Sawai and S. Yamada, *Astrophys. J.* 817, 153 (2016)
- [35] P. Msta, C. D. Ott, D. Radice, L. F. Roberts, E. Schnetter, & R. Haas, *Nature (London)* 528, 376 (2015)
- [36] T. Rembiasz, M. Obergaulinger, P. Cerd-Durn, E. Mller, & M. A. Aloy, *Mon. Not. Roy. Astron. Soc.* 456, 3782 (2016)
- [37] Mallick, R., Schramm, S., *Phys. Rev. C* 89, 025801 (2014)
- [38] Csernai, L. P., *Zh. Eksp. Teor. Fiz.* **92**, 379 (1987)
- [39] Serot, B. D., & Walecka, J. D., *Adv. Nucl. Phys.* 16, 1 (1986)
- [40] Boguta, J., & Bodmer, R. A., *Nucl. Phys. A* 292, 413 (1977)
- [41] Glendenning, N. K., & Moszkowski, *Phys. Rev. Lett.* 67, 2414 (1991)
- [42] Lalazissis, G. A., Knig, J. & Ring, P., *Phys. Rev. C* 55, 540 (1997)
- [43] A. Chodos, R. L. Jaffe, K. Johnson, C. B. Thorn & V. F. Weisskopf, *Phys. Rev. D* 9, 3471 (1974)
- [44] Mallick, R., and Schramm, S., *Phys. Rev. C* 89, 045805 (2014)
- [45] Bandyopadhyay, D., Chakrabarty, S., Dey, P., & Pal, S., *Phys. Rev. D*, 58, 121301 (1998)
- [46] Dexheimer, V., Negreiros, R., & Schramm, S., *Eur. Phys. J. A*, 48, 189 (2012)
- [47] Taub, A. H., *Phys. Rev.* 74, 328 (1948)

- [48] de Hoffmann, F., & Teller, E., Phys. Rev. **80**, 692 (1950)
- [49] L. D. Landau & E. M. Lifshitz, Fluid Mechanics (Pergamon Press, 1987)